Interpretation of the Sulfation Rate of CaO, MgO, and ZnO with SO_2 and SO_3

Published models for gas-solid reactions have been used with certain modifications to interpret sulfation data for CaO, MgO, and ZnO with SO_2 and SO_3. None of the models evaluated gave an adequate interpretation for high solid conversions, which were found to exceed 90% in some cases. Such high conversions are inconsistent with the current models, and a new mechanism must be postulated to explain the reaction after the solid product theoretically fills the initial pores of the particle. An important factor in successfully interpreting the experimental data is the distributed nature of the pore sizes within the solid particle.

Duygu Kocaefe, Deniz Karman, F. R. Steward
Department of Chemical Engineering
University of New Brunswick
Fredericton, N.B., Canada E3B 5A3

Introduction

The reaction of sulfur dioxide with various basic oxides has received considerable attention as this reaction is one method of removing sulfur dioxide from stack gas. A similar reaction that has received less attention is the reaction of sulfur trioxide with various basic oxides. The basic oxides on which most studies have been carried out are CaO and MgO because these materials are inexpensive, they have a high reactivity, and the disposal of the sulfate products is relatively easy.

The overall reaction between the sulfur oxides and the basic oxides can be represented by the general forms

$$MO(s) + SO_3(g) \rightarrow MSO_4(s)$$
$$MO(s) + SO_2(g) + \tfrac{1}{2}O_2(g) \rightarrow MSO_4(s) \qquad (1)$$

where M represents Ca, Mg, Zn, or possibly other less common basic metals.

The reaction between the gas and the solid occurs within the porous solid oxide particles. Numerous studies have been made on the rate of reaction of mixtures of SO_2 and O_2 in fixed and fluidized beds as well as in small-scale thermogravimetric laboratory reactors (Borgwardt and Harvey, 1972; Dogu, 1981; Hartman and Coughlin, 1974; Hartman et al., 1978; Ingraham and Marier, 1971). Recent work by Kocaefe et al. (1985) gives a substantial amount of data on the reaction of CaO, MgO, and ZnO with SO_3. A commensurate amount of theoretical work has gone into the development of mathematical models to interpret the laboratory data (Bhatia and Perlmutter, 1981; Christman and Edgar, 1983; Georgakis et al., 1979; Hartman and Trnka, 1980; Lindner and Simonsson, 1981; Ramachandran and Smith, 1977). Ramachandran and Doraiswamy (1982) give a comprehensive review of models proposed for noncatalytic gas-solid reactions. Certain of these models have been applied to the sulfation reactions under investigation here for the low range of solid conversions (30–50%) only. For example, the data of Borgwardt and Harvey (1972) and Hartman and Coughlin (1974) have been used by numerous authors to verify proposed models.

This study has extended the time of reaction so that solid conversions as high as 90% were achieved. It was found that the current models could not predict such high conversions in a reliable manner. A modification to the models was made that allowed the reaction to continue after the surface pores were filled with reaction product. This allowed a correlation of the data in this high conversion range. Solid diffusivities for SO_2 and SO_3 within particles of CaO, MgO, and ZnO were determined from the data based on the various models. The mechanism by which a particle of CaO can react beyond the complete filling of all pores within the particle with $CaSO_4$ remains to be explained.

General Analysis of Gas-Solid Reactions

The physical factors that dominate the behavior of this kind of reaction are the formation of a solid product layer through which the gaseous reactants must diffuse in order to react with the solid reactant, and the structural change of the solid particles that take place as the reaction proceeds. One factor that contributes to the structural change of the solid particles is the difference in molar volumes of the solid reactant and product quantified by the ratio

$$\alpha = \frac{V_{\text{product}}}{V_{\text{reactant}}}$$

Correspondence concerning this paper should be addressed to Deniz Karman.

Table 1. General Equations for Various Gas-Solid Reaction Models

Model	r_e		$d\bar{r}_2/d\bar{t}$		ϵ	$X(R,t)$
	Before Pore Plugging	After Pore Plugging	Before Pore Plugging	After Pore Plugging		
CGSM	$\dfrac{\phi^2\bar{r}_2^2\beta\bar{C}}{\beta+\bar{r}_2(1-\bar{r}_2/\bar{r}_1)}$	$\phi^2\bar{r}_2^2\bar{C}$	$-\dfrac{\beta\bar{C}}{\beta+\bar{r}_2(1-\bar{r}_2/\bar{r}_1)}$	$-\bar{C}$	$\dfrac{1-\epsilon}{1-\epsilon_o}=\bar{r}_1^3$	$1-\bar{r}_2^3$
	$\phi^2=\dfrac{3\tau(1-\epsilon_o)kR_o^2}{r_oD_{MK}\epsilon_o}$		$\bar{t}=t/(r_o/kC^oV)$			
	$\beta=D_s/kr_o$		$\bar{t}=0\quad\bar{r}_1=\bar{r}_2=1$			
CPSM	$\dfrac{\phi^2\bar{r}_2\bar{C}}{1+\dfrac{\bar{r}_2}{\beta}\ln\dfrac{\bar{r}_2}{\bar{r}_1}}$	$\phi^2\bar{r}_2\bar{C}$	$\dfrac{\bar{C}}{1+\dfrac{\bar{r}_2}{\beta}\ln\dfrac{\bar{r}_2}{\bar{r}_1}}$	$\bar{C}$	$\dfrac{\epsilon}{\epsilon_o}=\bar{r}_1^2$	$\dfrac{\bar{r}_2-\bar{r}_1^2}{\alpha}\dfrac{\epsilon_o}{1-\epsilon_o}$
	$\phi^2=\dfrac{2k\tau R_o^2}{r_oD_{MK_{t=0}}}$		$\bar{t}=t/(r_o/kC^oV)$	$\bar{r}_1=0$		
	$\beta=D_s/kr_o$		$\bar{t}=0\quad\bar{r}_1=\bar{r}_2=1$			
PSSM	$\dfrac{\phi^2\bar{C}}{\dfrac{S_0}{S_2}+\dfrac{LS_0}{\ell_o\beta S_{av}}}$	$\phi^2\dfrac{S_2}{S_0}C$	$-\dfrac{S_0}{S_2}\dfrac{\bar{C}}{\dfrac{S_0}{S_2}+\dfrac{LS_0}{\ell_o\beta S_{av}}}$	$-\bar{C}$	$\dfrac{1-\epsilon}{1-\epsilon_o}=\dfrac{F(\bar{r}_i,\lambda)}{F(r_o,\lambda)}$	$1-\dfrac{F(\bar{r}_2,\lambda)}{F(r_o,\lambda)}$
	$\phi^2=\dfrac{R_okS_0\tau}{D_{MK}\epsilon_o}$		$\bar{t}=0\quad\bar{r}_1=\bar{r}_2=1$ $\bar{t}=t/(r_o/kVC^o)$ $i=0,1,2$		$F(\bar{r}_i,\lambda)=\bar{r}_i^3-\dfrac{n}{4}(\bar{r}_i-\lambda^2)(2\bar{r}_i+\lambda)\quad$ for $\bar{r}_2>\lambda$	
	$\beta=D_s/k\ell_o$		$F(\bar{r}_2,\lambda)=\bar{r}_2^3\quad$ for $\bar{r}_2<\lambda$			
	$\ell_o=3(1-\epsilon_o)/S_o$					
	$S_i=\dfrac{3(1-\epsilon_o)[2\bar{r}_i-nf(\bar{r}_1,\lambda)]}{r_o\left[2-n(1-\lambda)^2\left(1+\dfrac{\lambda}{2}\right)\right]}$					
	$i=0,1,2$					
	where $f(\bar{r}_i,\lambda)=\bar{r}_i(\bar{r}_i-\lambda)\quad$ for $i=0,1$ $f(\bar{r}_2,\lambda)=\bar{r}_2(\bar{r}_2-\lambda)\quad\bar{r}_2>\lambda$ $0\quad\bar{r}_2\leq\lambda$					
	$S_{av}=\sqrt{S_1S_2}$					
RPM	$\dfrac{\phi^2\bar{C}}{\dfrac{S_0}{S_2}+\dfrac{LS_0}{\ell_o\beta S_{av}}}$	$\phi^2\dfrac{S_2}{S_0}\bar{C}$	$\dfrac{S_0}{S_2}\dfrac{\bar{C}}{\dfrac{S_0}{S_2}+\dfrac{LS_0}{\ell_o\beta S_{av}}}$	$\bar{C}$	$\dfrac{\epsilon}{\epsilon_o}=\bar{r}_1^2\left(\dfrac{G-\bar{r}_1}{G-1}\right)$	$\dfrac{\epsilon_o}{1-\epsilon_o}\left(\bar{r}_2^2\dfrac{G-\bar{r}_2}{G-1}-1\right)$
	$\phi^2=\dfrac{R_o^2kS_0\tau}{D_{MK_{t=0}}\epsilon_o}$		$\bar{t}=0\quad\bar{r}_1=\bar{r}_2=1$			
	$\beta=D_s/k\ell_o$					
	$S_i=\dfrac{\epsilon_o}{r_o}\dfrac{(2G-3\bar{r}_i)\bar{r}_i}{(G-1)}$		$\bar{t}=t/(r_o/kVC^o)$			
	$i=0,1,2$					
	$S_{av}=\dfrac{S_1-S_2}{\ln S_1/S_2}$					
DPM	$\dfrac{R_o^2 2k\tau}{D_{MK_{t=0}}}\sum_k\dfrac{\bar{r}_{2k}/r_{o_k}\eta_k}{1+\dfrac{\bar{r}_{2k}}{\beta_k}\ln\dfrac{\bar{r}_{2k}}{\bar{r}_{1k}}}$	$\dfrac{R_o^2 2k\tau}{D_{MK_{t=0}}}\sum_k\dfrac{\bar{r}_{2k}}{r_{o_k}}\eta_k$	$\dfrac{(\bar{r}_{2k}/\bar{r}_{1k})\bar{C}}{1+\dfrac{\bar{r}_{2k}}{\beta_k}\ln\dfrac{\bar{r}_{2k}}{\bar{r}_{1k}}}$	$\bar{C}$	$\dfrac{\epsilon_k}{\epsilon_{o_k}}=\bar{r}_1$	$\dfrac{\epsilon_o}{(1-\epsilon_o)\alpha}\sum_k\eta_k(\bar{r}_{2k}-\bar{r}_{1k})$
	$\beta_k=D_s/r_{o_k}k$		$\bar{t}=0\quad\bar{r}_{1k}=\bar{r}_{2k}=1$ $\bar{t}=t/(r_{o_k}/kC^oV)$	$\bar{r}_{1k}=0$	$\epsilon_o=\Sigma\epsilon_o\eta_k$	

For the sulfation reactions under investigation $\alpha > 1.0$, and a considerable effort has been made to describe the physical changes of a particle as the reaction occurs. Linder and Simonsson (1981) provide a detailed review of the various types of changes in the particle structure during the reaction proposed by previous workers.

Most of the mathematical models assume that the solid particles are porous to the reactant gas and are spherical in shape. For such a case a material balance on the reactant gas penetrating the particle is given by

$$\frac{1}{\bar{R}^2}\frac{\partial}{\partial \bar{R}}\left(\bar{R}^2 \bar{D}_{\text{eff}}\frac{\partial \bar{C}}{\partial \bar{R}}\right) = r_e \tag{2}$$

where r_e, the local rate of reaction per unit volume, is a function of time and radial position within the particle. Inherent in the writing of Eq. 2 is the assumption that the accumulation of the reactant gas within the pores of the particle is negligible relative to the rate of reaction with the solid, the pseudosteady-state approximation.

The boundary conditions for the particle are

$$\bar{R} = R_0 \qquad \bar{C} = 1 \tag{3a}$$

$$\bar{R} = 0 \qquad \frac{\partial \bar{C}}{\partial \bar{R}} = 0 \tag{3b}$$

The boundary condition in Eq. 3a assumes that the resistance to mass transfer from the external gas to the surface of the particle is negligible.

The effective diffusivity of gaseous reactant into the particle accounts for the porosity and tortuosity of the particle via

$$D_{\text{eff}} = \frac{\epsilon D_{mk}}{\tau} \tag{4}$$

although the inclusion of tortuosity is not particularly useful due to lack of independent data. The D_{mk} term accounts for both molecular and Knudsen diffusion by

$$\frac{1}{D_{mk}} = \frac{1}{D_k} + \frac{1}{D_m} \tag{5}$$

The effective diffusivity is normalized by using its initial value ($\epsilon = \epsilon_o$) and decreases linearly with porosity as the reaction proceeds.

The local reaction rate per unit volume, r_e, on the righthand side of Eq. 2 must be defined in terms of particle parameters, reactant gas concentration, and temperature. The various gas-solid reaction models make different assumptions regarding the nature of this term. The models described in this paper can be divided into two categories, depending on the manner in which the particle is characterized:

1. Models that describe the solid phase of the particle
2. Models that describe the pore space within the particle

Each model is described briefly below in qualitative terms indicating the physical makeup of the particle. The mathematical equations resulting from the physical descriptions are tabulated in Table 1.

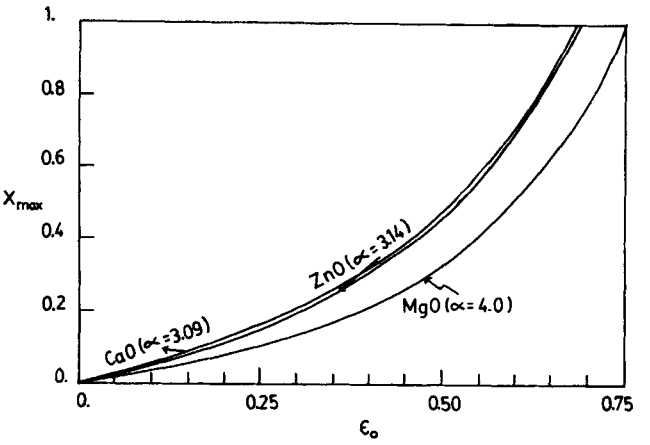

Figure 1. Dependence of limited conversion on initial particle porosity.

Description of Models

Changing grain size model (CGSM)

The CGSM of Georgakis et al. (1979) assumes that the spherical particle is made up of small spherical "grains" that are nonporous. The grains are characterized by an initial radius. Since $\alpha > 1$, the radius of the grains increases and the radius of the unreacted core decreases as the reaction proceeds. The rate of reaction of the grains is determined by two resistances in series: the diffusion through the product layer and the reaction at the surface of the unreacted core.

Partially sintered spheres model (PSSM)

The PSSM of Lindner and Simonsson (1981) takes into account that the individual grains are not spherical. An individual grain is assumed to be in contact with a number of neighboring grains; this is quantified by a sintering parameter. The spherical symmetry of the grains is thus perturbed and the unreacted core is not equally accessible from all directions. The equations describing this model are similar to those of the CGSM although algebraically somewhat more complicated. The formulations include the surface area of the grains and the number of neighboring grains contacting each individual grain.

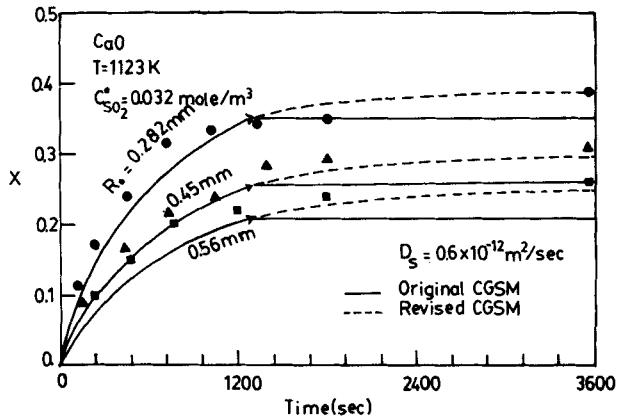

Figure 2. Fractional conversion vs. time, CaO/SO_3.
Curves: Changing grain size model predictions
Symbols: Data of Hartman and Coughlin (1974)

Table 2. Parameters Used for Simulation of Data from Present Study

	ZnO	MgO	CaO
ϵ_o, Initial porosity	0.65	0.67	0.51
Pore radius, m	0.232×10^{-6}	0.2×10^{-6}	0.975×10^{-6}
Grain radius, m	0.2×10^{-6}	0.2×10^{-6}	$1. \times 10^{-6}$
Molar volume, m^3/mol	0.1451×10^{-4}	0.1105×10^{-4}	0.169×10^{-4}
$\alpha = \frac{\text{molar volume sulfate}}{\text{molar volume oxide}}$	3.14	4.0	3.09

However, there is only one additional parameter, the degree of sintering, since the other parameters can be related to the initial radius and the sintering parameter through the particle porosity.

Changing pore size model (CPSM)

The CPSM, Kocaefe (1986), assumes that the particle consists of numerous pores of given initial radius and length. The reaction rate can thus be related to the consideration of a single representative pore. Since $\alpha > 1$, as the reaction proceeds the radius of the pore decreases and the radius of the unreacted solid surface increases. As the reaction proceeds the solid product will eventually fill the pore. The rate of reaction within the particle is determined by these three processes.

Random-pore model (RPM)

The RPM of Lindner and Simonsson (1981) assumes that the particle consists of a network of randomly intersecting pores. The intersection of the pores requires further geometric analysis. An initial pore length is introduced as an additional parameter. However, this parameter can be related to the surface area of the pores through the particle porosity.

Distributed-pore model (DPM)

The DPM of Christman and Edgar (1983) and Kocaefe (1986) assumes that the particle consists of numerous pores of a given size distribution, all in contact with the surface. The pores are assumed not to intersect internally. The pore size distribution can be represented by a continuous function or a discrete function. The reaction product builds up within the pores and eventually fills them, as in the CPSM.

Table 3. Simplified Pore Size Distribution Used for Distributed-Pore Model

η	r_o, m
MgO	
0.246	0.198×10^{-7}
0.446	0.885×10^{-7}
0.16	0.245×10^{-6}
0.148	0.6×10^{-6}
CaO	
0.12	0.172×10^{-7}
0.35	0.366×10^{-6}
0.40	0.125×10^{-5}
0.13	0.267×10^{-5}
ZnO	
0.652	0.82×10^{-7}
0.348	0.52×10^{-6}

Concept of limited conversion

In all the above models it is assumed that the volume of the solid particle remains constant. As the reaction proceeds the less dense product fills the pore space within the particle. Therefore, a "limited conversion" exists at the point at which no additional pore space remains. This limited conversion, X_{max}, can be calculated from the relation

$$X_{max}(1 - \epsilon_o)(\alpha - 1) = \epsilon_o \tag{6}$$

Figure 1 presents the limited conversion vs. initial porosity for CaO, MgO, and ZnO based on the values of α for the conversion to their respective sulfates.

Since the concentration of reactant gas will always be the maximum value at the particle surface, the rate of reaction will be favored at this point. This must therefore result in the filling of the pores at the particle surface at a time earlier than at points in the interior. Some models have assumed that the reaction ceases when the pores at the surface are filled. This results in a conversion considerably lower than that given by Eq. 6.

In this study the models described above have been modified to allow the reaction within the particle to continue after the pores are filled with product at the surface. This is achieved by allowing diffusion through the solid product layer after the surface pores are filled. In all cases the radius of the particle was assumed constant. These modifications allow the reaction rate to proceed beyond the point at which the pores become filled with reaction product at a reduced rate. With these modifications the models are more consistent with the experimental data.

The data for the sulfation of ZnO and MgO achieved conversions equal to or slightly greater than the limited conversion given by Eq. 6 under some experimental conditions. However, certain experimental conditions for the sulfation of CaO yielded conversions as high as 90%, which is significantly greater than the 50% calculated from Eq. 6 based on the appropriate initial

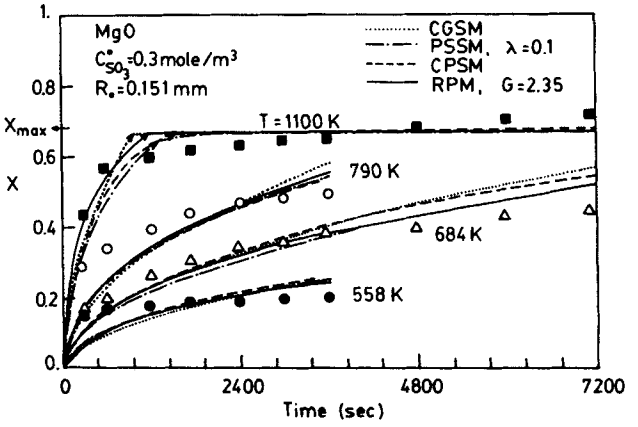

Figure 3. Fractional conversion vs. time, MgO/SO_3.
Curves: Model predictions
Symbols: Experimental data

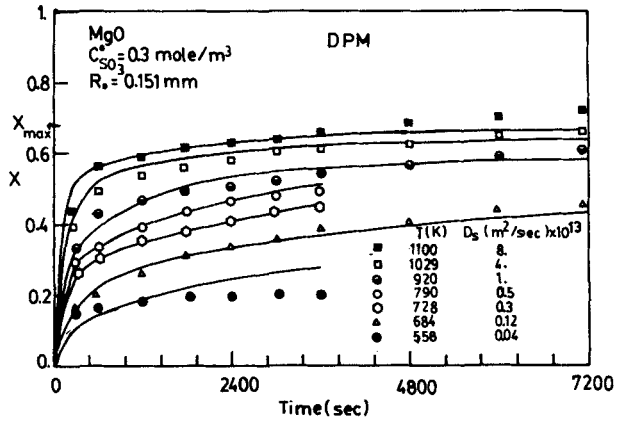

Figure 4. Fractional conversion vs. time, MgO/SO_3, temperature as variable.
Curves: Distributed-pore model predictions
Symbols: Experimental data

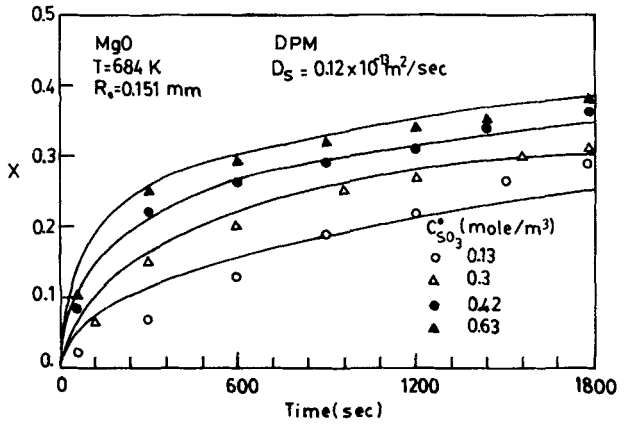

Figure 6. Fractional conversion vs. time, MgO/SO_3, gaseous reactant concentration as variable.
Curves: Distributed-pore model predictions
Symbols: Experimental data

porosity. In order for the particle to accommodate this conversion the diameter would have to increase by 14%, certainly a significant change.

By allowing the reaction within the particle to continue after the surface pores are filled with product, the models are able to predict the conversion at extended reaction times more reliably. Figure 2 demonstrates this improvement for the CGSM for the data of Hartman and Coughlin 1974. The modification eliminates the somewhat artificial "pore plugging time" suggested by the original models. The limited conversion given by Eq. 6 for these data is 54% (ϵ_o = 0.52, α = 3), well above the values observed for 3,600 s.

Numerical procedure

The systems of equations presented in Table 1 were solved by a finite-difference technique using a backward difference method. The nondimensional particle radius was divided into 20 sections and a nondimensional time step of 0.1 was used. These values were found to give a solution that was within 2% of the values obtained from smaller increments. The computer code was prepared in modular form so that the different models could be accommodated by using the appropriate set of modules for each case while retaining the modules common to all cases. Some workers (Georgakis et al., 1979) prefer to use an orthogonal collocation technique, which is claimed to be numerically more efficient for a particular model calculation. The finite-difference technique with the various modules is believed to be more convenient for the numerous models used in this comparison because of the large investment of effort required in formulating the mathematics for the orthogonal collocation scheme.

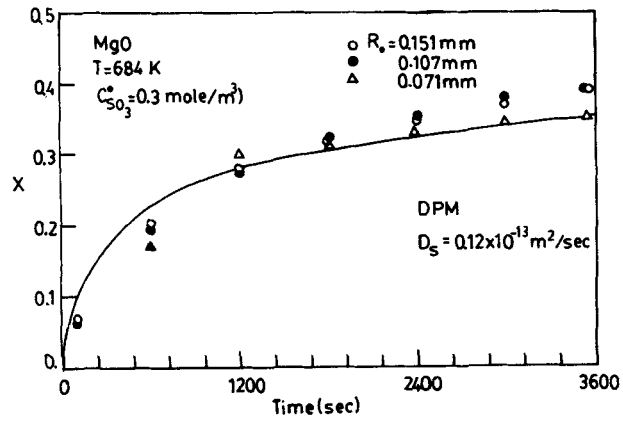

Figure 5. Fractional conversion vs. time, MgO/SO_3, particle radius as variable.
Curve: Distributed-pore model prediction
Symbols: Experimental data

Interpretation of Data

The experimental details and original data have been reported previously (Kocaefe et al., 1985). A thermogravimetric apparatus was used to conduct experiments for various particle radii (0.071–0.151 mm), temperatures (450–1,100 K), and con-

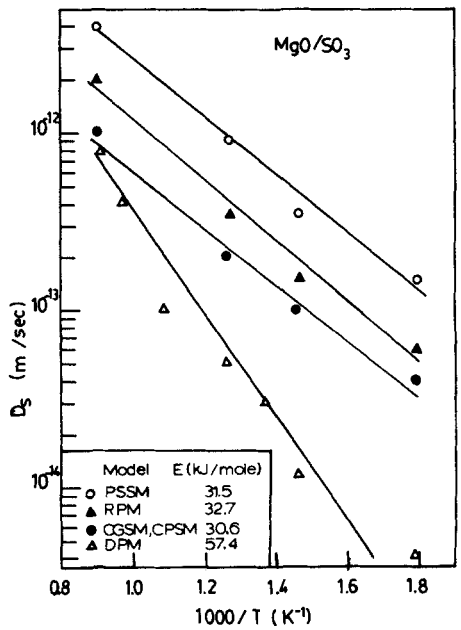

Figure 7. Arrhenius plot: model predictions of temperature dependence of D_s for MgO/SO_3.

centrations of SO_2 or SO_3 (0.075–0.62 mol/m^3) and O_2 (0.0–1.5 mol/m^3). Measurements also provide particle grain and pore radii, porosity, and pore size distribution. Table 2 lists the solid reactant characteristics that have been used in all model calculations. Characteristics that vary among runs are indicated in the appropriate figures. Table 3 gives the pore size distribution for the three samples used.

Using values in Table 2 and the properties of the gases involved, the molecular and Knudsen diffusivities of the gaseous reactant have been expressed as functions of temperature using standard equations (Fuller et al., 1966).

The rate constant for the reaction at the surface of the unreacted solid appears in all of the models. There is considerable variation reported in the literature for these rates, for example, from 4.2×10^{-4} to 6.6×10^{-2} m/s for CaO reacting with SO_2 at 1,123 K. (Hartman and Coughlin, 1976; Christman and Edgar, 1983; Wen and Ishida, 1973). For the cases under investigation here, the overall reaction rate is insensitive to variations in the value of the rate constant of these magnitudes. The key parameter in fitting the models to the data is therefore the diffusivity of the gaseous reactant through the product layer. In the discussion that follows, this single parameter has been adjusted so that the models can be made to agree with the data.

MgO data

Figure 3 demonstrates the interpretation of four sets of MgO sulfation data at different temperatures with four of the models presented. The values of D_s used for the CGSM and CPSM are identical. The values of D_s required for the PSSM and RPM to obtain good agreement with the data are higher than those for the CGSM and CPSM. It is clear that the quality of agreement with the data is comparable among these models.

The computed curves emphasize the reaction rate at higher conversions (longer times) relative to the rate at lower conversions (shorter times) when compared with the data. At the highest temperature (and final conversion) the fit is best although the computed curves cross the data at two points. At lower temperatures (and final conversions) the discrepancy mentioned above is more pronounced. The data show an asymptotic approach to a final conversion that seems to be a function of temperature, whereas the model computations approach the same final conversion, albeit more slowly at lower temperatures. Of the inputs to the model calculations, the pore or grain sizes are admittedly the most difficult to measure accurately as these quantities are in the submicron range. The effect of a change in this input on the model calculations is to change the value of D_s that must be used to obtain agreement with the data. The qualitative aspects of the agreement with the data described above are not affected.

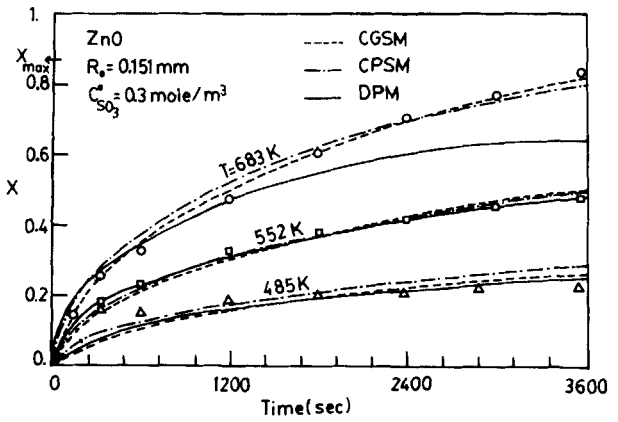

Figure 8. Fractional conversion vs. time, ZnO/SO_3, temperature as variable.

Curves: Model predictions
Symbols: Experimental data

Model	D_s, m^2/s $\times 10^{12}$, at 683 K	552 K	485 K
CGSM	0.3	0.11	0.03
CPSM	0.35	0.11	0.035
DPM	0.08	0.03	0.008

In marked contrast to the four models presented in Figure 3, the distributed-pore model gives a much better representation of the data, as shown in Figure 4. Data at other intermediate temperatures are also included here to give a complete picture. The agreement with the data at the lowest temperature is not much of an improvement over those in Figure 3, but at all other temperatures the data are represented well with the calculated curves.

Particle size and gaseous reactant concentration are the two other experimental parameters that were used in the study. Figures 5 and 6 show the effects of these parameters on the progress of reaction at an intermediate temperature. In the range of particle radii studied (71–150 μm) the conversion vs. time data for different radii were hardly distinguishable and the model calculations concur, showing no effect of resistance due to diffusion into the particle. The effects of gas composition over a modest range (0.13–0.63 mol/m^3) are significant and reasonably well interpreted by the calculated curves.

The temperature dependency of the solid diffusivity predicted by all models is shown in Figure 7. The D_s values and the activation energies for four of the models are similar, given the uncertainties in determining the values from the data. The DPM shows a significantly higher activation energy as well as generally lower values for D_s.

ZnO data

Interesting contrasts are observed here relative to the interpretation of MgO data. Figure 8 shows calculations for CGSM

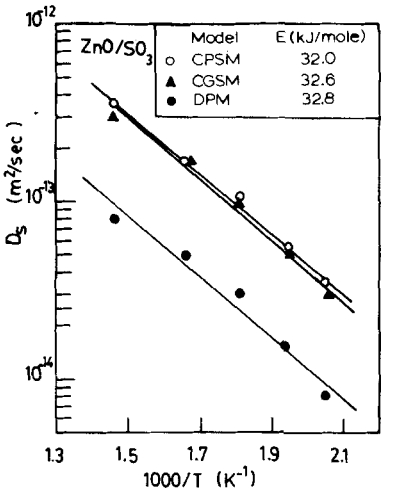

Figure 9. Arrhenius plot: model predictions of temperature dependence of D_s for ZnO/SO_3.

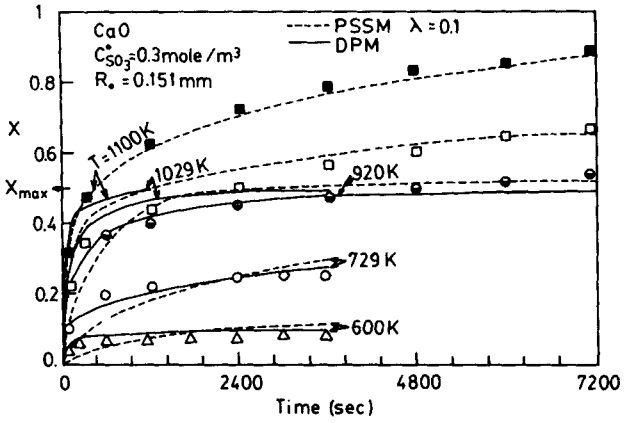

Figure 10. Fractional conversion vs. time, CaO/SO_3, temperature as variable.
Curves: Partially sintered spheres model and distributed-pore model predictions
Symbols: Experimental data

Model	1,100 K	1,029 K	D_s, m²/s 920 K	729 K	600 K
PSSM	0.1×10^{-7}	0.2×10^{-8}	0.28×10^{-10}	0.35×10^{-11}	0.5×10^{-12}
DPM	0.12×10^{-9}	0.4×10^{-10}	0.2×10^{-10}	0.7×10^{-12}	0.3×10^{-13}

and CPSM in comparison with ZnO data at three different temperatures. All are in a lower temperature range compared to MgO due to the low melting point of ZnO. Momentarily leaving aside the topmost curve for DPM, all three models give good agreement with the data, much better for CGSM and CPSM compared to the MgO case.

The improvement can be explained by the differences in physical structure between the MgO and ZnO samples used. The ZnO showed a much more uniform structure than MgO both in pore size distribution and in electron micrographs. For MgO the DPM gives a better agreement than other models because it accounts for the nonuniformity of pore sizes, while for ZnO with a uniform structure it has no advantage over the other models. The topmost curve for DPM levels off around 60% conversion due to significant pore closure at the particle surface. The other two models continue to higher conversions. The activation energies for the three models are similar although the D_s values are lower for the DPM, as shown in Figure 9.

CaO data

An important characteristic of the data on the sulfation of CaO with SO_3 and $SO_2 + O_2$ mixtures obtained in our study was the very high conversions reached at high temperatures when the runs are sufficiently long. Conversions as high as 90% cannot be interpreted without assuming major structural changes of the particle. The approach taken here is to use the empirical modification to the grains or pores mentioned earlier, but to allow the particle to continue to react beyond the limited conversion determined from Eq. 6.

The results of this approach are demonstrated by the PSSM curves in Figure 10, which shows data for CaO at seven different temperatures. The high-temperature data that exceed the limited conversion of 50% are well represented by this modified PSSM. At lower temperatures the discrepancy between the model curves and the data is of the same type as for MgO, the model curves exhibiting a tilt relative to the data.

The DPM, on the other hand, provides a much better repre-

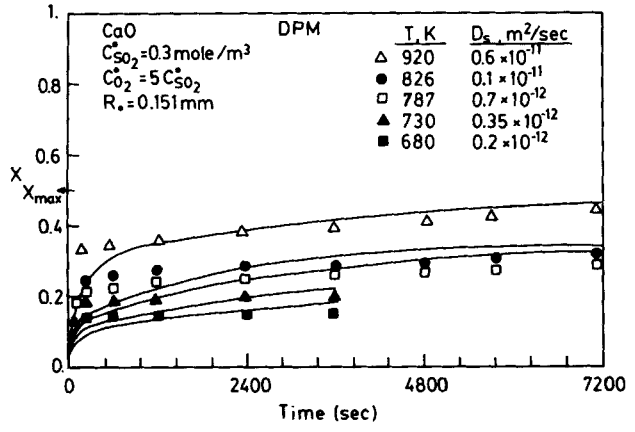

Figure 11. Fractional conversion vs. time, $Cao/SO_2 + O_2$, temperature as variable.
Curves: Distributed-pore model predictions
Symbols: Experimental data

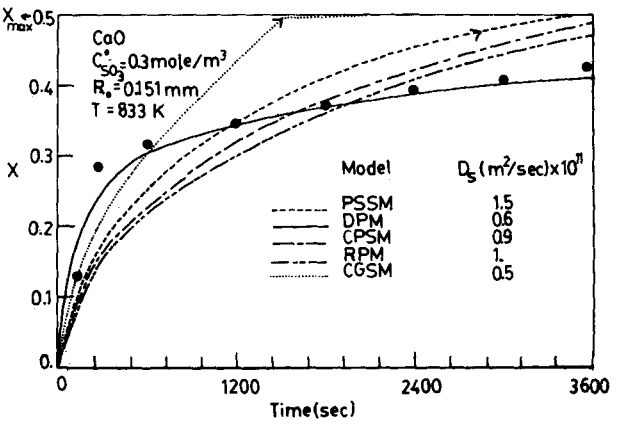

Figure 12. Fractional conversion vs. time, CaO/SO_3 at 833 K.
Curves: Model predictions
Symbols: Experimental data

sentation of the data throughout the range of conversions up to 50%, the "limited conversion." It fails, however, to represent conversions above this value. Almost identical trends are shown in Figure 11 by data for $SO_2 + O_2$ as the gaseous reactant. The CaO sample used also had a significant pore size distribution measured by mercury intrusion porosimetry and shows nonuniformity based on electron microscopy. One would thus expect the DPM to give a better representation of the data.

A comparison of all the models discussed is given in Figure 12 for one set of CaO-SO_3 data. Except for the DPM curve all calculations are plagued with the imbalance between the behavior at low and high conversions mentioned earlier. The temperature dependency of D_s for CaO data with both gaseous reactants is shown in Figure 13. This figure indicates that the D_s for CaO has the highest activation energy for sulfation with SO_3 among the three materials studied.

Discussion

The diffusivity of gaseous reactant in the solid product layer is the process that dominates the overall rate of reaction between the metal oxides and sulfur oxides in this study. This process is also the least understood aspect of gas-solid reactions. In all gas-solid reaction models the diffusivity D_s is simply the proportionality constant between flux and the driving concentration difference across the product layer. In the absence of a means for direct measurement or prediction, D_s becomes the parameter by which agreement is sought between model predictions and data. In this study, it was shown that when determining D_s qualitative agreement between model and data is not always satisfactory, and the apparent D_s values are strongly influenced by the idealizations used in characterizing the solid particles.

This is reflected in the magnitudes of D_s values calculated from different models for the same data, and has been noted previously by Christman and Edgar (1983), who point to the wide range (6×10^{-13}–3×10^{-10} m^2/s) of values reported by various workers for SO_2 through $CaSO_4$ at 850°C.

The temperature dependency of the solid diffusivity is also of interest for understanding the nature of the governing process.

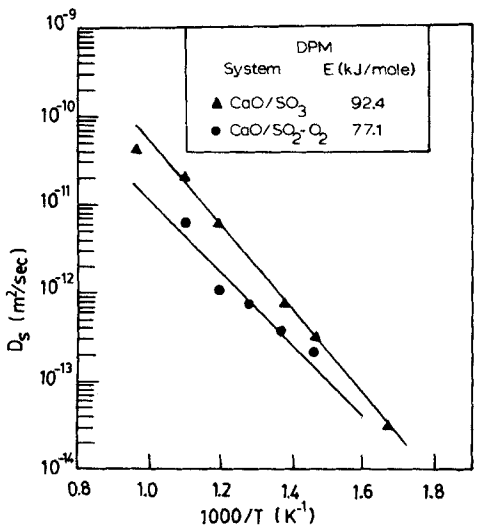

Figure 13. Arrhenius plot: distributed-pore model predictions of temperature dependence of D_s for $CaO/SO_2 + O_2$ and CaO/SO_3.

In many cases limited data have been used to demonstrate the suitability of models, and activation energies have not been reported. Christman and Edgar report 120 kJ/mol and note that this is similar to ionic migration in the solid phase. Hartmann and Trnka (1980) report 142 kJ/mol and note the lack of data for independent verification. The activation energies deduced in this study are considerably lower than these figures and point to the possibility of different mechanisms. Christman and Edgar mention the possibility of forming microscale cracks during the formation of the product layer. If the gaseous reactant follows such a path the activation energy of the process would naturally be lower. It is, however, premature to speculate on the significance of the observed activation energies unless the D_s values can be obtained from a more satisfactory representation of the data by the models. The most important result of this study has been to show that none of the models previously tested against data taken over a limited range can provide an adequate representation for the data collected in this study covering wide ranges of temperature and solid conversion.

If the solid particles have a distribution of pore sizes it is imperative that this distribution be taken into account as in the distributed-pore model. Even this case fails to represent solid behavior when solid conversion exceeds the theoretical maximum governed by initial porosity and the parameter α. The modifications to the models given in this study provide improved representations of the data in some cases. However, these modifications are not based on any physical description of what happens inside the particle after pore closure at the surface. A general model for the sulfation of metal oxides should therefore incorporate postulations about changes in the particles as a whole, as well as local changes in grain or pore size as the reaction proceeds.

Notation

C^o = initial gas concentration, mol/m^3
C = gas concentration, mol/m^3
$\bar{C}$ = dimensionless gas concentration
D_k = Knudsen diffusivity m^2/s
D_m = molecular diffusivity m^2/s
D_{mk} = transition region diffusivity, m^2/s
D_s = product layer diffusivity, m^2/s
D_{sff} = effective diffusivity, m^2/s
$\bar{D}_{eff}$ = dimensionless effective diffusivity
E = activation energy, kJ/mol
G = parameter characterizing the RPM
k = reaction rate constant based on unit reaction surface area, m/s
L = product layer thickness, m
ℓ_o = characteristic distance for PSSM and RPM
R_o = particle radius, m
$\bar{R}$ = dimensionless radial distance in particle
r_e = dimensionless reaction rate based on particle volume
r_o = initial average grain or pore radius, m
$\bar{r}_1$ = dimensionless pore or grain radius
$\bar{r}_2$ = dimensionless position of reaction interface in pore or grain
r_{ok} = initial average pore radius for kth region of pore size distribution in DPM, m
$\bar{r}_{1_k}$ = dimensionless pore radius for kth region of pore size distribution in DPM
$\bar{r}_{2_k}$ = dimensionless position of reaction interface in pore for kth region of pore size distribution in DPM
S_0 = initial specific surface area, m^{-1}
S_1 = specific surface area of product layer, m^{-1}
S_2 = specific surface area of reaction interface, m^{-1}
S_{av} = average specific surface area for diffusion, m^{-1}
t = time, s

$\bar{t}$ = dimensionless time
V = molar volume, m^3/mol
X = solid conversion
X_{max} = maximum theoretical limit for solid conversion

Greek letters

α = molar volume ratio of solid product to solid reactant
β = ratio of product layer diffusivity to product of reaction rate constant and characteristic length in model
ϵ = porosity
ϵ_o = initial porosity
η_k = ratio of pore volume of kth region to total pore volume in DPM
λ = ratio of distance between contact point and grain center to initial grain radius in PSSM
τ = tortuosity
ϕ = Thiele modulus

Literature Cited

Bhatia, S. R., and D. D. Perlmutter, "The Effect of Pore Structure on Fluid-Solid Reactions: Application to the SO_2-Lime Reaction," *AIChE J.*, **27**, 226 (1981).

Borgwardt, R. H., and R. D. Harvey, "Properties of Carbonate Rocks Related to SO_2 Reactivity," *Envir. Sci. Technol.*, **6**, 350 (1972).

Christman, P. G., and T. F. Edgar, "Distributed Pore-Size Model for Sulfation of Limestone," *AIChE J.*, **29**, 388 (1983).

Dogu, T., "The Importance of Pore Structure and Diffusion in the Kinetics of Gas-Solid Noncatalytic Reactions: Reaction of Calcined Limestone with SO_2," *Chem. Eng. J.*, **21**, 213 (1981).

Fuller, E. N., P. D. Schettler, and J. C. Giddings, "A New Method for Prediction of Binary Gas Phase Diffusion Coefficients," *Ind. Eng. Chem.*, **58**, 19 (1966).

Georgakis, C., C. W. Chang, and J. Szekely, "A Changing Grain Size Model for Gas-Solid Reactions," *Chem. Eng. Sci.*, **34**, 1072 (1979).

Hartman, M., and R. W. Coughlin, "Reaction of Sulfur Dioxide with Limestone and the Influence of Pore Structure," *Ind. Eng. Chem. Process Des. Dev.*, **13**, 248 (1974).

———, "Reaction of Sulfur Dioxide with Limestone and the Grain Model," *AIChE J.*, **22**, 490 (1976).

Hartman, M., J. Pata, and R. W. Coughlin, "Influence of Porosity of Calcium Carbonates on Their Reactivity with Sulfur Dioxide," *Ind. Eng. Chem. Process Des. Dev.*, **17**, 411 (1978).

Hartman, M., and O. Trnka, "Influence of Temperature on the Reactivity of Limestone Particles with Sulfur Dioxide," *Chem. Eng. Sci.*, **35**, 1189 (1980).

Ingraham, T. R., and P. Marier, "Mechanism of the Absorption of SO_2 by Limestone," *J. Air Pollut. Contr. Ass.*, **21**, 347 (1971).

Kocaefe, D., "An Experimental and Theoretical Study on the Kinetics of Basic Oxide Sulfation with SO_2 and SO_3," Ph.D. Thesis, Chem. Eng. Dept., Univ. New Brunswick, Fredericton, Canada (1986).

Kocaefe, D., D. Karman, and F. R. Steward, "Comparison of the Sulfation Rates of Calcium, Magnesium, and Zinc Oxides with SO_2 and SO_3," *Can. J. Chem. Eng.*, **63**, 971 (1985).

Lindner, B., and D. Simonsson, "Comparison of Structural Models for Gas-Solid Reactions in Porous Solids Undergoing Structural Changes," *Chem. Eng. Sci.*, **36**, 1519 (1981).

Ramachandran, P. A., and L. K. Doraiswamy, "Modeling of Noncatalytic Gas-Solid Reactions," *AIChE J.*, **28**, 881 (1982).

Ramachandran, P. A., and J. M. Smith, "Effect of Sintering and Porosity Changes on Rates of Gas-Solid Reactions," *Chem. Eng. J.*, **14**, 137 (1977).

Wen, C. Y., and M. Ishida, "Reaction Rate of Sulfur Dioxide with Particles Containing Calcium Oxide," *Environ. Sci. Technol.*, **7**, 703 (1973).

Manuscript received Feb. 21, 1986, and revision received Mar. 9, 1987.